JOURNAL OF GUIDANCE, CONTROL, AND DYNAMICS
Vol. 33, No. 3, May–June 2010

Spin-Axis Attitude Determination Using In-Flight Data

Jozef C. van der Ha*
Kyushu University, Fukuoka 819-0395, Japan

DOI: 10.2514/1.46811

The paper presents a practical spin-axis attitude determination approach based on the Tanygin–Shuster algorithm. The technique is illustrated by means of sensor measurement data originating from two satellites with very different orbit and attitude characteristics. The most appropriate data intervals are identified using criteria based on measurement sensitivities. A minimum-variance technique is formulated for establishing the Earth aspect angle from the measured chord angles. The chain of covariance transformations from the fundamental sensor measurement errors to the final attitude error is presented. The unit-vector normalization technique, which is an inherent part of the Tanygin–Shuster method, is found to be beneficial for the stability of the attitude determination results under unknown biases, especially in cases in which only a subset of the measurement angles are available.

Introduction

SPIN-STABILIZATION offers a straightforward, cost-effective, as well as robust attitude control concept for many satellite mission applications. A combination of sun and Earth sensors is often used to provide the two independent reference directions required by the attitude determination algorithms. The determination of the spin-axis attitude orientation is usually achieved by the application of a batch least-squares estimation method using the available sensor measurements [1].

This paper illustrates the practical application of the Tanygin–Shuster (T-S) algorithm [2] for spin-axis attitude estimation. This method is based on a linear measurement model for the functional relationship between the sensor measurements and the spin-axis attitude and includes zero-mean Gaussian measurement noise. It delivers the maximum-likelihood estimate of the spin-axis attitude that minimizes the sum of the weighted squares of the measurement residuals.

A unique and valuable aspect of the Tanygin–Shuster algorithm is the manner in which the unit-vector constraint for the spin-axis attitude orientation is incorporated. The application of Lagrange's method of multipliers leads to a straightforward iteration technique to determine the multiplier as well as the resulting unit-vector attitude estimate.

This study employs actual sensor measurements from two satellites with very different orbit and attitude characteristics. The first application uses data generated by the CONTOUR satellite [3] near the end of its Earth-phasing orbits about two days before its ill-fated injection into a heliocentric trajectory on 15 August 2002. CONTOUR's phasing orbits have unique characteristics [4], for instance, the perigee and apogee distances are 200 km and 116,000 km, respectively, and the orbital period is almost 42 h.

CONTOUR's Earth-sensor pencil beams have simultaneous Earth coverage over the altitude range from about 50,000 to 65,000 km. These joint coverage intervals start at about 36 h from perigee (i.e., after the apogee passage). The spin axis is oriented close to the direction of the perigee velocity vector. The specific mountings of the pencil beams at 60 and 65 deg cause the Earth aspect angle (i.e., the angle between the spin axis and the spacecraft-to-Earth direction) to decrease from about 65 to 58 deg during the sensor coverage interval [3].

Presented as Paper 127 at the AAS/AIAA Space Flight Mechanics Meeting, Savannah, GA, 8–12 February 2009; received 20 August 2009; revision received 29 November 2009; accepted for publication 29 November 2009.

*Professor, Department of Aeronautics & Astronautics.

The second set of sensor measurements originates from the METEOSAT Second Generation (MSG-2) satellite [5] during its near-geostationary drift phase in December 2005. The METEOSAT meteorological satellites have a spin-axis attitude orientation that points close to the orbit normal. Therefore, the Earth-sensor pencil beams have uninterrupted coverage throughout the orbit and the Earth aspect angle remains close to 90 deg, usually within a fraction of a degree.

The first task in the sensor data processing concerns the selection of appropriate data intervals based on our understanding of the data quality. This involves the assessment of the variations of the measurement sensitivities during the Earth-sensor coverage intervals. Singularities in the measurement functions occur at times when the partial derivatives of the Earth aspect angle with respect to the measured half-chord angles approach infinity. In the vicinity of these singularities, the measurement errors are magnified enormously when calculating the Earth aspect angle. Therefore, the elimination of measurements in the vicinity of these singularities enhances the quality of the resulting attitude estimate.

The input measurement covariances are established from the specified noise characteristics of the sensor measurements. In practice, the algorithm's performance is not very sensitive to the values of the noise as long as they are "realistic." A more serious challenge is presented by the unknown biases in the measurement data [6]. The bias effects are clearly visible in the measurement residuals and they are different for the two selected satellite applications.

The practical implementation of the T-S algorithm for spin-axis attitude determination is relatively straightforward. Only a few seconds of MATLAB® execution time are needed for data intervals of a number of hours. The sensor measurement data may contain any combination of sun aspect angles, Earth aspect angles, as well as sun–Earth dihedral angles. A difficult issue in spin-axis attitude determination is the derivation of the Earth aspect angle from the half-chord-angle measurements. A minimum-variance technique for the calculation of the Earth aspect angle will be presented here. The results show that the algorithm performances are different for the two satellites because of the different manifestations of the relevant biases (mainly caused by variations in the Earth's infrared radius).

Concerning the unit-vector normalization, a few interesting performance characteristics have been observed. In particular, in cases in which only two of the three measurement angles are used, the observability of the attitude vector is weakened and the performance of the attitude determination algorithm degrades under the influence of the unknown biases. The application of the unit-vector normalization procedure shows significant benefits in this case because it forces the attitude estimate closer to its actual direction.

Finally, we draw attention to a recent comprehensive technique for spin-axis attitude determination proposed by Markley and Sedlak [7]. They use an Extended Kalman Filter with a seven-parameter state vector based on angular-momentum properties and illustrate its practical implementation for a few NASA missions.

Summary of Tanygin: Shuster Estimator

The T-S attitude estimation technique [2] considers a set of N measurement vectors $\mathbf{y}_k$ generated at discrete, but not necessarily equidistant, instants of time t_k ($k = 1, \ldots, N$). The unknown spin-axis orientation is represented by the unit vector $\hat{\mathbf{z}}$ where the caret symbol denotes a unit vector. The functional relationship between the measurements $\mathbf{y}_k$ and $\hat{\mathbf{z}}$ is described by the linear system of measurement equations:

$$\mathbf{y}_k = H_k\hat{\mathbf{z}} + \mathbf{v}_k \qquad (k = 1, \ldots, N) \tag{1}$$

The measurement noise vector $\mathbf{v}_k$ is assumed to be modeled by a zero-mean white Gaussian process with measurement covariance matrices $R_k = E\{\mathbf{v}_k\,\mathbf{v}_k^T\}$.

The maximum-likelihood estimate $\hat{\mathbf{z}}^*$ for the attitude unit vector is the one that minimizes the cost function $J(\hat{\mathbf{z}})$ defined by

$$J(\hat{\mathbf{z}}) = \frac{1}{2}\sum_{k=1}^{N}(\mathbf{y}_k - H_k\hat{\mathbf{z}})^T R_k^{-1}(\mathbf{y}_k - H_k\hat{\mathbf{z}}) \tag{2}$$

This cost function can readily be rewritten in the form

$$J(\hat{\mathbf{z}}) = J_0 + \mathbf{G}^T\hat{\mathbf{z}} + \tfrac{1}{2}\hat{\mathbf{z}}^T F\hat{\mathbf{z}} \tag{3}$$

with

$$J_0 = \frac{1}{2}\sum_{k=1}^{N}\mathbf{y}_k^T R_k^{-1}\mathbf{y}_k \tag{4a}$$

$$\mathbf{G} = -\sum_{k=1}^{N} H_k^T R_k^{-1}\mathbf{y}_k \tag{4b}$$

$$F = \sum_{k=1}^{N} H_k^T R_k^{-1} H_k \tag{4c}$$

The scalar $J_0 = J(\mathbf{z} = \mathbf{0})$ is independent of the attitude vector. The column vector $\mathbf{G}$ is the gradient of $J(\mathbf{z})$ at $\mathbf{z} = \mathbf{0}$, and F is the symmetric Hessian matrix of $J(\mathbf{z})$ at $\mathbf{z} = \mathbf{0}$. The quantities $\mathbf{G}$ and F represent the individual measurements and covariances, respectively. The formulation in Eqs. (3) and (4) lead to a compact representation of the estimation problem at hand.

When we ignore the unit-vector constraint, we can readily establish the *unconstrained* attitude vector $\mathbf{z}_{\text{uc}}$ (which, in general, is not a unit vector) that minimizes the cost function $J(\mathbf{z})$:

$$\mathbf{z}_{\text{uc}} = -F^{-1}\mathbf{G} \tag{5}$$

We assume here that the matrix F is nonsingular, so that the inverted matrix is well defined.

In the case in which we take account of the unit-vector constraint, the Lagrange multiplier method may be used. An iteration technique can be applied for calculating the multiplier λ. Starting with $i = 0$ and $\lambda_0 = 0$, the iteration scheme for $i = 1, 2, \ldots$ proceeds as follows [1]:

$$D_i = (F + \lambda_i I_{3\times 3})^{-1} \tag{6a}$$

$$\mathbf{z}_i = -D_i\mathbf{G} \tag{6b}$$

$$\lambda_{i+1} = \lambda_i - \frac{(1 - \mathbf{z}_i^T\cdot\mathbf{z}_i)}{2(\mathbf{z}_i^T D_i\mathbf{z}_i)} \tag{6c}$$

It can be seen that $\mathbf{z}_0 = \mathbf{z}_{\text{uc}}$ as expected. In most cases, only one or two iterations are needed to establish the unit-vector attitude estimate $\hat{\mathbf{z}}^*$ with sufficient precision. The expressions for the covariance matrices of the unit vector $\hat{\mathbf{z}}^*$ can be found in [1].

Measurement Equations for Spin-Axis Attitude

Geometrical Background of Sensor Measurements

Figure 1 shows the geometry of the sun and Earth unit vectors $\mathbf{S}$ and $\mathbf{E}$ and the spin-axis attitude $\mathbf{Z}$. (In the rest of the paper, we denote the attitude unit vector by $\mathbf{Z}$, without caret). A typical V-slit sun sensor for spinning satellites has a vertical and a skew slit. The sun's crossing times over these slits are measured by silicon photo-detectors. Successive vertical slit crossings provide the spin-rate measurements. Successive crossings of the vertical and skew slits produce the sun aspect angle ϑ (Wertz [8], Sec. 7.1.1). The angle ϑ is the most common attitude measurement for spinning satellites and represents the angle between the spin axis and the sun direction (see Fig. 1):

$$\vartheta = \arccos\{\mathbf{Z}\cdot\mathbf{S}\} \tag{7}$$

The typical Earth sensor for spinning satellites has two static pencil beams that are oriented at the angles μ_i ($i = 1, 2$) relative to the spin axis (Fig. 1). The sensor outputs are produced by bolometer detectors measuring the Earth radiation in the CO_2 band of the infrared part of the spectrum. This band is selected because of its limited radiance variability under seasonal and weather influences (Wertz [8], Sec. 4.2).

The instants at which the Earth-sensor pencil-beam detectors cross the space/Earth (S/E) and Earth/space (E/S) boundaries are established by onboard signal processing. These crossing pulses represent the fundamental Earth-sensor measurements for downlink in the telemetry data. With our knowledge of the spin rate, we can express these pencil-beam crossing pulses in the half-chord angles κ_i ($i = 1, 2$). These are the fundamental Earth-sensor measurement angles to be used by the attitude determination algorithms. The spherical geometry in the triangle formed by the vectors $\mathbf{Z}$ and $\mathbf{E}$ and the directions of the S/E or E/S pulses (see Fig. 1) produce the relationship between the measured half-chord angles κ_i ($i = 1, 2$), the Earth aspect angle β, and the apparent Earth-radius angle ρ (Wertz [8], Eq. 11.7):

$$\cos\mu_i\cos\beta + \sin\mu_i\cos\kappa_i\sin\beta = \cos\rho \qquad (i = 1, 2) \tag{8}$$

The angle $\rho = \arcsin(R_E/r)$ represents the angle of the Earth's circular radius R_E seen by the satellite at orbital distance r. The Earth aspect angle β is defined as the angle between the spin axis $\mathbf{Z}$ and the spacecraft-to-Earth unit vector (or simply the Earth vector) $\mathbf{E}$ shown in Fig. 1:

$$\beta(\nu) = \arccos\{\mathbf{Z}\cdot\mathbf{E}(\nu)\} \tag{9}$$

The Earth vector $\mathbf{E}$ points opposite to the instantaneous orbital radius vector and rotates along with the satellite's orbital phase angle ν. Its evolution is known from orbit determination.

Figure 2 shows an example of the (simulated) half-chord angles κ_i ($i = 1, 2$) as a function of the Earth aspect angle. These results represent the nominal half-chord angles during the final part of

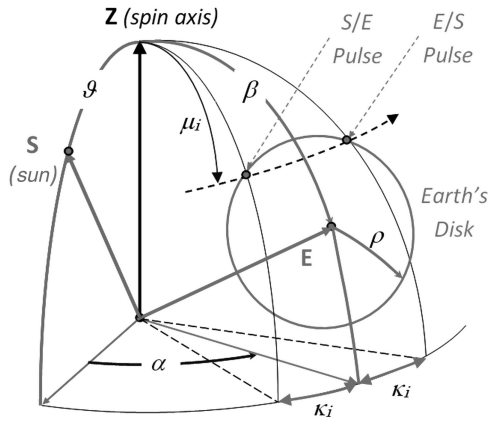

Fig. 1 Geometry of sun, Earth, spin axis, and measurements ϑ, β, and α.

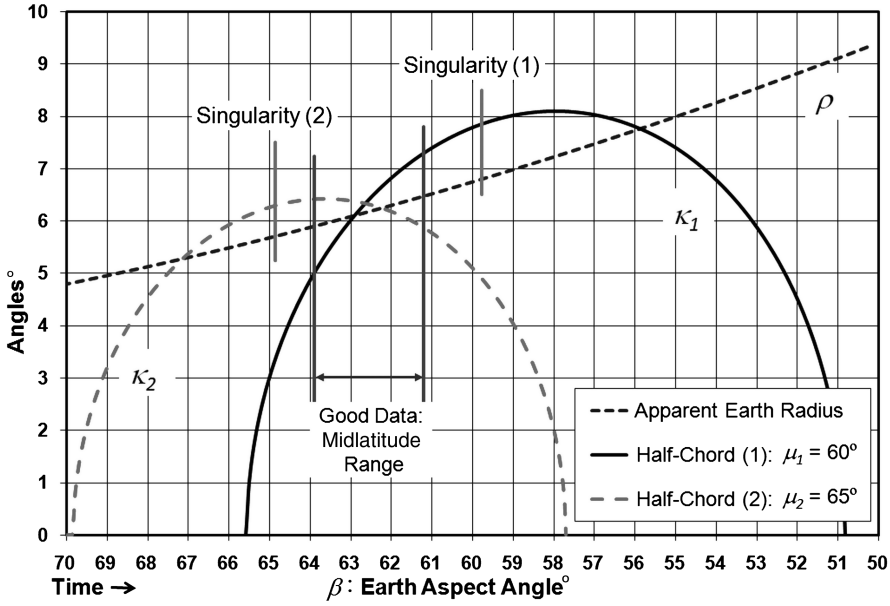

Fig. 2 Evolution of half-chord angles κ_i and Earth-radius angle ρ (CONTOUR).

CONTOUR's phasing orbits [3]. The implicit relationship in Eq. (8) represents the starting point for calculating the Earth aspect angle β from the measured half-chord angles κ_i. An explicit analytical result for the Earth aspect angle as a function of κ_1 and κ_2 is given in Eq. 28 of [5] with validity over the interval during which both pencil beams have simultaneous Earth coverage. The result in [5] is useful for a geostationary satellite with continuous Earth-sensor coverage (i.e., spin-axes orientation close to the orbit normal). Here, we deal with elliptical orbits and short Earth-sensor coverage intervals. We present an approach that is more suitable for the present application and also for the subsequent covariance analyses.

The best conditions in terms of the resulting attitude determination accuracy occur when the pencil beams scan the so-called midlatitude regions of the Earth corresponding to latitude bands between about 10 and 40 as well as -10 and $-40°$. It should be noted that the concept of "latitude" used here refers to the characteristics of the pencil-beam scans and is not necessarily identical to the familiar geographical Earth latitude. The combined midlatitude regions for both pencil beams under the nominal injection attitude conditions would correspond to Earth aspect angles in the range from about 61 to 64° as shown in Fig. 2. The results in Fig. 3 show that the sensitivity of the Earth aspect angles to the chord-angle measurement errors is below 1 in this region.

Determination of Earth Aspect Angle

We write the implicit Eq. (8) in a different form to facilitate the extraction of the Earth aspect angle β:

$$b_i \cos \nu_i \cos \beta + b_i \sin \nu_i \sin \beta = \cos \rho \qquad (i = 1, 2) \tag{10}$$

with the auxiliary functions b_i and ν_i defined as

$$b_i = \sqrt{1 - (\sin \mu_i \sin \kappa_i)^2} \qquad (i = 1, 2) \tag{11a}$$

$$\nu_i = \arctan\{\tan \mu_i \cos \kappa_i\} \qquad (i = 1, 2) \tag{11b}$$

Each of the pencil beams can be seen to produce its own two Earth-aspect-angle solutions:

$$\beta_i^{\pm} = \nu_i \pm \gamma_i \qquad (i = 1, 2) \tag{12a}$$

with

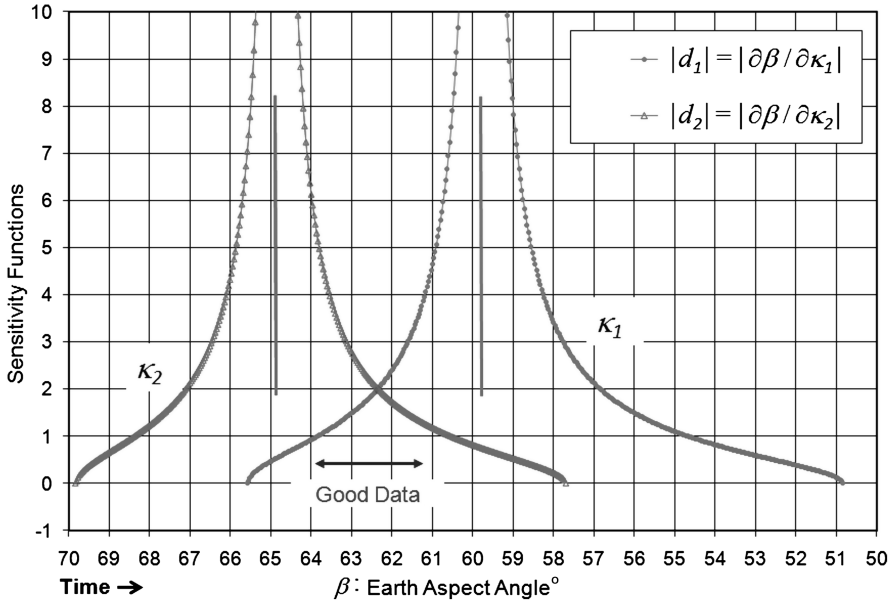

Fig. 3 Evolution of the sensitivity functions d_i ($i = 1, 2$) over combined coverage interval.

$$\gamma_i = \arccos\{(\cos\rho)/b_i\} \qquad (i = 1, 2) \tag{12b}$$

This result is useful for interpreting the behavior of the half-chord angles κ_i as functions of the Earth aspect angle β. In particular, when the angle κ_i vanishes, we find $\beta_i^{\pm} = \mu_i \pm \rho$ from Eqs. (11) and (12). These are the extreme Earth aspect angles that correspond to the start and end of the Earth-sensor coverage interval. On the other hand, when the angle γ_i in Eq. (12b) vanishes, the two $\beta_i^{\pm}$ angles coincide with the same value $\beta_i^* = \nu_i^*$ (with different values for the two pencil beams $i = 1, 2$) and we have $b_i^* = \cos\rho_i^*$. The expression in Eq. (11a) shows that the half-chord angles at these locations are $\kappa_i^* = \arcsin\{(\sin\rho_i^*)/\sin\mu_i\}$, $i = 1, 2$.

With the help of Eq. (8) we can show that the specific Earth aspect angles β_i^*, $i = 1, 2$, correspond to the locations where the half-chord angles κ_i reach their stationary or extreme values as functions of the Earth aspect angle, that is, $\partial\kappa_i/\partial\beta = 0$ at $\beta = \beta_i^*$, for $i = 1, 2$, while keeping the Earth-radius angle ρ fixed. These two singularities are shown in Figs. 2 and 3 for each of the two pencil beams. It is important to note that the extremes of the two chord angles as functions of the Earth aspect angle, that is, $\kappa_i(\beta)$ with $i = 1, 2$, are in general not identical to the locations where the pencil beams scan the Earth at its maximum width. This is because the evolution of the chord angles is also affected by the variations in the apparent Earth-radius angle.

For points away from the maximum chords, a particular value of κ_i may correspond to two Earth aspect angle values $\beta_i^{\pm}$, which is evident from Figs. 1 and 2. The geometry in Fig. 1 indicates that β_i^+ in Eq. (12a) corresponds to scans below the center of the Earth's disk and the solution β_i^- refers to scans above the Earth's center.

At the start and end of the pencil-beam coverage intervals, where $\kappa_i \approx 0$ ($i = 1, 2$), we find from Eqs. (11a) and (11b) that $b_i \approx 1$ and $\nu_i \approx \mu_i$. Equations (12a) and (12b) indicate that $\gamma_i = \rho$ and $\beta_i^{\pm} = \mu_i \pm \rho$ in these cases. Figure 1 shows that the zeros of the half-chord angles correspond to the maximum and minimum boundary values of the Earth aspect angle.

Error Sensitivity of Earth Aspect Angle

We explore the possibility of combining the two β_i solutions produced by the two pencil-beam chord measurements ($i = 1, 2$) into a single definitive Earth aspect angle β. The sensitivities of the two β_i solutions to the errors of the κ_i measurement angles vary significantly under the changing geometry during the respective Earth coverage intervals. Therefore, it is natural to use the individual sensitivity functions as criteria for the selection of the weights for the two β_i solutions. Such a technique offers the possibility to minimize the variance of the resulting β solution (at each point in the combined coverage interval) through the appropriate choice of the weights.

The sensitivity relationships of the variations in the Earth aspect angle β_i with respect to changes in the measured half-chord angles κ_i follow from Eq. (8):

$$d_i = \frac{\partial\beta_i}{\partial\kappa_i} = \frac{g_i}{h_i} \qquad (i = 1, 2) \tag{13a}$$

$$\Rightarrow \Delta\beta_i \approx d_i\Delta\kappa_i \qquad (i = 1, 2) \tag{13b}$$

Here, Δx denotes the error in the variable x and the functions g_i and h_i are defined as

$$g_i = \sin\kappa_i \tan\mu_i \tan\beta_i \qquad (i = 1, 2) \tag{14a}$$

$$h_i = \tan\mu_i \cos\kappa_i - \tan\beta_i \qquad (i = 1, 2) \tag{14b}$$

It can be seen that singularities occur, that is, $d_i \to \infty$, when the functions h_i ($i = 1, 2$) vanish. These singularities correspond precisely to the points $\beta_i^* = \nu_i^*$, for $i = 1, 2$, defined in Eq. (11b) and addressed in the preceding section.

Figure 3 shows the evolutions of the sensitivity functions d_1 and d_2, which have been established from the chord measurements over the combined sensor coverage intervals shown in Fig. 2. The singularities for the two chord measurements occur at the points $\beta_i^* = \nu_i^*$, where the half-chord angles κ_i are stationary as functions of the Earth aspect angle. At these points, the chord-length measurements cannot observe variations in the Earth aspect angle β and are thus of no use for the determination of the Earth aspect angle. It can be seen in Fig. 2 that the singularities do not coincide with the maximum chord lengths. This is because of the influence of the varying apparent Earth radius.

Optimal Earth Aspect Angle

The optimal (in a minimum-variance sense) Earth aspect angle estimate β^* will be established as the combination of the two individual β_i angles ($i = 1, 2$), which are obtained from the κ_i measurements as outlined in Eqs. (10–12). When introducing the weight w_1, we can write

$$\beta^* = w_1\beta_1 + (1 - w_1)\beta_2 \tag{15}$$

We express the error of β in terms of the half-chord-angle errors by means of Eq. (13b):

$$\Delta\beta \approx w_1 d_1\Delta\kappa_1 + (1 - w_1)d_2\Delta\kappa_2 \tag{16}$$

The two half-chord measurements κ_1 and κ_2 originate from different bolometer sensors and can be assumed to be independent so that the variance of β can be expressed as

$$\sigma_\beta^2 \approx E\{(\Delta\beta)^2\} = w_1^2 d_1^2\sigma_{\kappa_1}^2 + (1 - w_1)^2 d_2^2\sigma_{\kappa_2}^2 \tag{17}$$

We assume that the half-chord measurements are collected in the midlatitude region shown in Fig. 2. These regions are far away from the Earth's rim; therefore, we may assume that the covariances of the two κ_i measurements are essentially identical. Finally, we write Eq. (17) as

$$\sigma_\beta^2 \approx \{w_1^2 d_1^2 + (1 - w_1)^2 d_2^2\}\sigma_\kappa^2 \tag{18}$$

When differentiating this result with respect to the weight w_1, we obtain the following relationship:

$$\frac{\partial\sigma_\beta^2}{\partial w_1} = 2\{w_1 d_1^2 - (1 - w_1)d_2^2\}\sigma_\kappa^2 \tag{19}$$

The variance of the angle β reaches its minimal value when the right-hand side vanishes:

$$w_1 = d_2^2/(d_1^2 + d_2^2) \tag{20a}$$

$$1 - w_1 = d_1^2/(d_1^2 + d_2^2) \tag{20b}$$

After substituting these results into Eq. (18), we can express the expected error σ_β of the Earth aspect angle β in terms of the half-chord-angle measurement error σ_k:

$$\sigma_\beta = D\sigma_\kappa \tag{21a}$$

with

$$D = |d_1 d_2|/\sqrt{d_1^2 + d_2^2} \tag{21b}$$

The function D denotes the magnification of the standard deviation of β relative to that of the κ_i angles.

Figure 4 shows the evolutions of the weighting functions w_i ($i = 1, 2$) and the ratio D. These results are calculated on the basis of the predicted chord measurements within the joint sensor coverage interval (see Fig. 2). At the start of the joint coverage interval (from about 36.2 to 37 h since perigee) the pencil beam 2 measurements are degraded due to the vicinity of its singularity. Therefore, the higher weights are assigned to the pencil beam 1 data, which yield the most accurate calculation of β. Closer to the end of the joint coverage interval (i.e., from 37.2 to 38.1 h), the situation is reversed and the pencil beam 2 measurements carry the higher weight.

The preference of the sensor measurements shifts from pencil beam 1 to pencil beam 2 in the middle of the range of "good" scans in

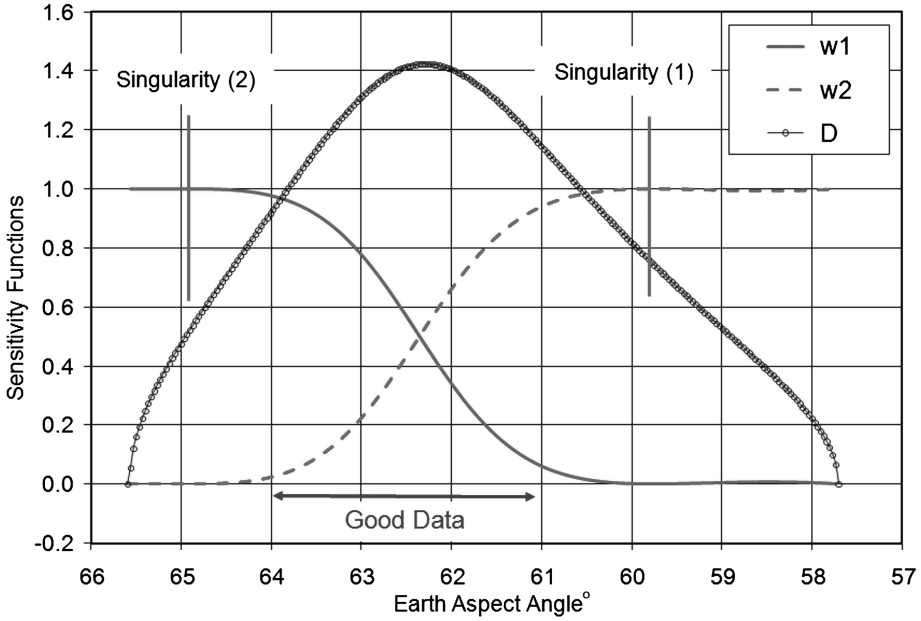

Fig. 4 Evolution of the weighting functions w_1, $w_2 = 1 - w_1$, and ratio D.

the Earth's midlatitude region. The point of equal weights is at about 37.1 h, which corresponds to an Earth aspect angle of about 62.4° in Fig. 4. Also, the maximum error ratio ($D \approx 1.42$) occurs here, and so the maximum Earth aspect angle error is about 40% larger than the half-chord-angle measurement noise.

Figure 4 indicates that the most favorable conditions for the calculation of the Earth aspect angle β would appear to occur near the start and end of the joint sensor coverage interval, that is, at about 36.2 and 38.1 h, corresponding to Earth aspect angles of 65.6 and 57.7°, respectively. The low error is due to the theoretically excellent sensitivity, that is, $d_i \approx 0$ at these locations. Unfortunately, the corresponding pencil-beam scans are very close to the Earth's rim here and have relatively large systematic errors that reduce their practical usefulness.

Optimal Sun–Earth Dihedral Angle

The geometry of the sun- and Earth-sensor measurements produces one more independent measurement, namely, the sun–Earth dihedral angle α. This rotation angle is proportional to the time interval between the sun crossing the sun sensor's vertical slit and the Earth sensor measuring the Earth-center crossing (Fig. 1). From spherical geometry within the triangle formed by the **S**, **E**, and **Z** unit vectors, we can establish the intricate measurement equation between α and **Z**, which also includes the other measurement angles ϑ and β:

$$\alpha(\nu) = \arcsin\{(\mathbf{S} \times \mathbf{E}) \cdot \mathbf{Z}/(\sin\vartheta \sin\beta)\} \tag{22}$$

In practice, each of the two pencil beams produces its own sun–Earth dihedral angle α_i ($i = 1, 2$). The measurements α_i are calculated as the average value of the time intervals between the sun crossing the sun sensor's vertical slit and each of the pencil-beam S/E and E/S pulses (Fig. 1). The establishment of the "optimal" angle α from the two independent α_i measurements is straightforward because the relevant measurement sensitivities are essentially identical for Earth-sensor measurements in the midlatitude range. Therefore, the two α_i measurements may be weighted equally:

$$\alpha = (\alpha_1 + \alpha_2)/2 \tag{23}$$

Establishment of Measurement Equations

We summarize the three fundamental measurement equations established in Eqs. (7), (9), and (22) as a system of three linear equations $\mathbf{y} = H\mathbf{Z}$:

$$\mathbf{y} = \begin{pmatrix} \cos\vartheta \\ \cos\beta \\ \sin\vartheta \sin\beta \sin\alpha \end{pmatrix} \tag{24a}$$

$$H = \begin{pmatrix} S_1 & S_2 & S_3 \\ E_1 & E_2 & E_3 \\ (\mathbf{S}\times\mathbf{E})_1 & (\mathbf{S}\times\mathbf{E})_2 & (\mathbf{S}\times\mathbf{E})_3 \end{pmatrix} \tag{24b}$$

The indices 1, 2, and 3 denote the components of the respective vectors in the geocentric inertial reference frame. As long as the reference vectors **S** and **E** are not aligned, the system $\mathbf{y} = H\mathbf{Z}$ is well defined and the matrix H can be inverted to produce the inertial attitude vector $\mathbf{Z} = H^{-1}\mathbf{y}$. This represents a so-called *single-frame* attitude solution because the three measurements are collected at a single instant of time. Because the attitude vector **Z** should be a unit vector, normalization must still be performed afterward, for instance, by the iteration technique in Eq. (6).

In practical applications [2], a batch of N measurements, $\vartheta_k, \beta_k, \alpha_k$ ($k = 1, \ldots, N$), will be collected over N spin revolutions. The system of equations now contains N times the system in Eqs. (24) for the three unknown components of the attitude **Z** and is thus overdetermined. We add the random errors $\mathbf{v}_k = (\nu_{1k}, \nu_{2k}, \nu_{3k})^T$ to each of the individual sets ($k = 1, \ldots, N$) of measurements $\mathbf{y}_k = (y_{1k}, y_{2k}, y_{3k})^T$ given in Eqs. (24a), which leads to the system of N vector equations:

$$\mathbf{y}_k = H_k\mathbf{Z} + \mathbf{v}_k \qquad (k = 1, 2, \ldots, N) \tag{25}$$

This leads immediately to the weighted-least-squares attitude estimate $\mathbf{Z}^*$:

$$\mathbf{Z}^* = F^{-1} \sum_{k=1}^{N} H_k^T R_k^{-1} \mathbf{y}_k \tag{26a}$$

$$\text{with } F = \sum_{k=1}^{N} H_k^T R_k^{-1} H_k \tag{26b}$$

It may be noted that the matrix F was introduced already in Eq. (4c) and that the expression in Eq. (26a) is equivalent to the unconstrained estimate of the T-S algorithm established in Eq. (5).

The measurement covariance matrix R_k represents the 3×3 random noise of the vector $\mathbf{y}_k$:

$$R_k = E\{\mathbf{v}_k\, \mathbf{v}_k^T\} = \begin{pmatrix} \sigma_1^2 & \sigma_{21} & \sigma_{13} \\ \sigma_{21} & \sigma_2^2 & \sigma_{23} \\ \sigma_{13} & \sigma_{23} & \sigma_3^2 \end{pmatrix}_k \tag{27}$$

It can be shown that the state covariance matrix is given by

$$Q = E\{\Delta\mathbf{Z}(\Delta\mathbf{Z})^T\} = F^{-1} \tag{28}$$

This result allows us to express the attitude errors in terms of the measurement errors via the matrix R_k in Eq. (27).

Calculation of Measurement Covariance Matrix

The fundamental measurements for attitude determination purposes are the six sun and Earth sensors crossing times t_j ($j = 0, \ldots, 5$). The first two, that is, t_0 and t_1, represent the sun-sensor crossings over the meridian and skew slits, respectively. The times t_2 and t_3 denote the S/E and E/S crossings of pencil beam 1 with mounting angle μ_1. Similarly, t_4 and t_5 are the S/E and E/S crossing times of pencil beam 2 with angle μ_2. The random errors in the crossing times t_j are written as Δt_j ($j = 0, \ldots, 5$) with expected values $E\{\Delta t_j\} = 0$ and covariances $E\{(\Delta t_j)^2\} = \sigma_j^2$ ($j = 0, \ldots, 5$).

Because the spin rate ω is known (from the running average of successive meridian slit crossings), it is easy to convert the crossing times t_j into the associated rotation angles τ_j ($j = 1, \ldots, 5$) with reference to the sun-sensor meridian slit's crossing time t_0:

$$\tau_j = \omega(t_j - t_0) \qquad (j = 1, \ldots, 5) \tag{29}$$

The random errors are $\Delta\tau_j = \omega(\Delta t_j - \Delta t_0) + (t_j - t_0)\Delta\omega$ with $j = 1, \ldots, 5$. The spin rate follows from a large number of measurements so that its random error may be considered negligible in a steady-state situation (in the absence of nutation and wobbling motion). After writing the angular errors in vector notation, that is, $\Delta\boldsymbol{\tau} = (\Delta\tau_1, \ldots, \Delta\tau_5)^T$, we can express their covariance matrix in the variances of t_j and t_0 with the help of Eq. (29) while noting that the individual measurements are uncorrelated, that is, $E\{(\Delta t_j \Delta t_0)\} = 0$ for $j = 1, \ldots, 5$ and $k = 0, \ldots, 5$:

$$T = E\{\Delta\boldsymbol{\tau}(\Delta\boldsymbol{\tau})^T\} = \omega^2 \begin{pmatrix} \sigma_1^2 + \sigma_0^2 & \sigma_0^2 & \sigma_0^2 & \sigma_0^2 & \sigma_0^2 \\ \sigma_0^2 & \sigma_2^2 + \sigma_0^2 & \sigma_0^2 & \sigma_0^2 & \sigma_0^2 \\ \sigma_0^2 & \sigma_0^2 & \sigma_3^2 + \sigma_0^2 & \sigma_0^2 & \sigma_0^2 \\ \sigma_0^2 & \sigma_0^2 & \sigma_0^2 & \sigma_4^2 + \sigma_0^2 & \sigma_0^2 \\ \sigma_0^2 & \sigma_0^2 & \sigma_0^2 & \sigma_0^2 & \sigma_5^2 + \sigma_0^2 \end{pmatrix} \tag{30}$$

Next, we introduce the vector of the measurement angles $\boldsymbol{\gamma} = (\vartheta, \kappa_1, \kappa_2, \alpha_1, \alpha_2)^T$. The sun aspect angle ϑ can be calculated from the inclination angle (denoted by i_S) between the vertical and skew slits and the measured rotation angle τ_1 (Wertz [8], Eq. 7-1):

$$\vartheta(\tau_1) = \pi/2 - \arctan\{\sin\tau_1 / \tan i_S\} \tag{31}$$

Therefore, the random error $\Delta\vartheta$ in the sun aspect angle is found as

$$\Delta\vartheta = g(\tau_1)\Delta\tau_1 \tag{32a}$$

$$\text{with}: \; g(\tau_1) = -\sin\vartheta(\tau_1)\cos\vartheta(\tau_1)/\tan\tau_1 \tag{32b}$$

This result loses validity when $\tau_1 \approx 0$, near the intersection of the vertical and inclined slits where $\vartheta \approx 90$ deg. In this case we may write $\varepsilon = \vartheta - \pi/2$ and use the approximate asymptotic result:

$$\Delta\vartheta = \Delta\varepsilon \approx -(\tan i_S)^{-1}\Delta\tau_1 \tag{33}$$

The half-chord angles κ_i and dihedral angles α_i (with $i = 1, 2$) are defined by the S/E and E/S crossings of the two pencil beams:

$$\kappa_1 = (\tau_3 - \tau_2)/2 \tag{34a}$$

$$\kappa_2 = (\tau_5 - \tau_4)/2 \tag{34b}$$

$$\alpha_1 = (\tau_3 + \tau_2)/2 \tag{34c}$$

$$\alpha_2 = (\tau_5 + \tau_4)/2 \tag{34d}$$

We can write these definitions in matrix form as $\Delta\boldsymbol{\gamma} = G\Delta\boldsymbol{\tau}$ with matrix G defined by

$$G = \frac{1}{2}\begin{pmatrix} 2g & 0 & 0 & 0 & 0 \\ 0 & -1 & 1 & 0 & 0 \\ 0 & 0 & 0 & -1 & 1 \\ 0 & 1 & 1 & 0 & 0 \\ 0 & 0 & 0 & 1 & 1 \end{pmatrix} \tag{35}$$

We find the covariance matrix Γ of the measurement angles $\boldsymbol{\gamma} = (\vartheta, \kappa_1, \kappa_2, \alpha_1, \alpha_2)^T$ with the help of Eqs. (30) and (35):

$$\Gamma = E\{\Delta\boldsymbol{\gamma}(\Delta\boldsymbol{\gamma})^T\} = GTG^T = \frac{\omega^2}{4}\begin{pmatrix} 4g^2(\sigma_0^2 + \sigma_1^2) & 0 & 0 & 4g\sigma_0^2 & 4g\sigma_0^2 \\ 0 & \sigma_2^2 + \sigma_3^2 & 0 & \sigma_3^2 - \sigma_2^2 & 0 \\ 0 & 0 & \sigma_4^2 + \sigma_5^2 & 0 & \sigma_5^2 - \sigma_4^2 \\ 4g\sigma_0^2 & \sigma_3^2 - \sigma_2^2 & 0 & 4\sigma_0^2 + \sigma_2^2 + \sigma_3^2 & 4\sigma_0^2 \\ 4g\sigma_0^2 & 0 & \sigma_5^2 - \sigma_4^2 & 4\sigma_0^2 & 4\sigma_0^2 + \sigma_4^2 + \sigma_5^2 \end{pmatrix} \tag{36}$$

For pencil-beam scans in the midlatitude region, we may assume that the random noise in the S/E and E/S crossing times of the two pencil beams are essentially equal so that $\sigma_2 \approx \sigma_3 \approx \sigma_4 \approx \sigma_5$. The noise effects in these crossing times are obviously also independent of each other. Furthermore, we assume that the random noise terms of the two sun-sensor slit crossing times are close to identical as well, that is, $\sigma_1 \approx \sigma_0$. Thus, Eq. (36) can be simplified further to its final form:

$$\Gamma = E\{\Delta\boldsymbol{\gamma}(\Delta\boldsymbol{\gamma})^T\} \approx \frac{\omega^2}{2}\begin{pmatrix} 4g^2\sigma_0^2 & 0 & 0 & 2g\sigma_0^2 & 2g\sigma_0^2 \\ 0 & \sigma_2^2 & 0 & 0 & 0 \\ 0 & 0 & \sigma_2^2 & 0 & 0 \\ 2g\sigma_0^2 & 0 & 0 & 2\sigma_0^2 + \sigma_2^2 & 2\sigma_0^2 \\ 2g\sigma_0^2 & 0 & 0 & 2\sigma_0^2 & 2\sigma_0^2 + \sigma_2^2 \end{pmatrix} \tag{37}$$

The angular measurements shown in Fig. 1, that is, $\boldsymbol{\eta} = (\vartheta, \beta, \alpha)^T$, can be expressed in terms of the vector $\boldsymbol{\gamma}$. In particular, the Earth aspect angle follows from the weighted combination of the individual solutions as defined in Eq. (15). The covariance transformation is based on the linearized transformation of the random errors $\Delta\kappa_i$ to $\Delta\beta$ as established in Eq. (16), and so we have

$$\Delta\boldsymbol{\eta} \approx W\Delta\boldsymbol{\gamma} \tag{38a}$$

with

$$W = \begin{pmatrix} 1 & 0 & 0 & 0 & 0 \\ 0 & w_1 d_1 & (1-w_1)d_2 & 0 & 0 \\ 0 & 0 & 0 & 0.5 & 0.5 \end{pmatrix} \tag{38b}$$

The parameters w_1 and $1 - w_1$ represent the weighting functions of the Earth aspect angles β_1 and β_2 for the two pencil beams. The optimal weights have been given in Eqs. (20) in terms of the individual measurement sensitivities. The expression for the covariance matrix of the angles $\boldsymbol{\eta}$ follows now as

$$B = E\{\Delta\boldsymbol{\eta}(\Delta\boldsymbol{\eta})^T\} = \frac{\omega^2}{4}\begin{pmatrix} 8g^2\sigma_0^2 & 0 & 4g\sigma_0^2 \\ 0 & 2D^2\sigma_2^2 & 0 \\ 4g\sigma_0^2 & 0 & 4\sigma_0^2 + \sigma_2^2 \end{pmatrix} = \begin{pmatrix} \sigma_\vartheta^2 & 0 & \sigma_{\vartheta\alpha} \\ 0 & \sigma_\beta^2 & 0 \\ \sigma_{\vartheta\alpha} & 0 & \sigma_\alpha^2 \end{pmatrix} \tag{39}$$

The covariance terms appearing in the right-hand matrix are defined by the corresponding expressions in the preceding matrix. The result in Eq. (39) shows that, under the fairly realistic assumptions spelled out here, the Earth aspect angle measurement β is uncorrelated to both the sun aspect angle ϑ and the sun–Earth dihedral angle α measurements. On the other hand, the sun aspect angle measurement ϑ obviously has a nonzero correlation to the α measurement.

Finally, we convert $\boldsymbol{\eta} = (\vartheta, \beta, \alpha)^T$ to the measurement observations $\mathbf{y}$ defined in Eqs. (24a). The linearized transformation matrix of the error components is given by

$$\Delta\mathbf{y} \approx F\begin{pmatrix} \Delta\vartheta \\ \Delta\beta \\ \Delta\alpha \end{pmatrix} \tag{40a}$$

with

$$F = \begin{pmatrix} -\sin\vartheta & 0 & 0 \\ 0 & -\sin\beta & 0 \\ f_\theta & f_\beta & f_\alpha \end{pmatrix} \tag{40b}$$

with auxiliary functions f_θ, f_β, and f_α defined by

$$f_\theta = \cos\vartheta \sin\beta \sin\alpha \tag{41a}$$

$$f_\beta = \sin\vartheta \cos\beta \sin\alpha \tag{41b}$$

$$f_\alpha = \sin\vartheta \sin\beta \cos\alpha \tag{41c}$$

The final result for the covariance matrix of $\mathbf{y}$ follows as

$$R = E\{\Delta\mathbf{y}(\Delta\mathbf{y})^T\} = FE\{\Delta\boldsymbol{\eta}(\Delta\boldsymbol{\eta})^T\}F^T = FBF^T = \begin{pmatrix} \sigma_1^2 & 0 & \sigma_{13} \\ 0 & \sigma_2^2 & \sigma_{23} \\ \sigma_{13} & \sigma_{23} & \sigma_3^2 \end{pmatrix} \tag{42}$$

The covariance elements in the matrix on the right-hand side are defined as follows:

$$\sigma_1^2 = \sigma_\theta^2 \sin^2\vartheta \tag{43a}$$

$$\sigma_2^2 = \sigma_\beta^2 \sin^2\beta \tag{43b}$$

$$\sigma_3^2 = f_\theta^2\sigma_\theta^2 + f_\beta^2\sigma_\beta^2 + f_\alpha^2\sigma_\alpha^2 + 2f_\theta f_\alpha \sigma_{\theta\alpha} \tag{43c}$$

$$\sigma_{13} = -(f_\theta\sigma_\theta^2 + f_\alpha\sigma_{\theta\alpha})\sin\vartheta \tag{43d}$$

$$\sigma_{23} = -f_\beta\sigma_\beta^2 \sin\beta \tag{43e}$$

These results complete the explicit calculation of the *measurement* covariance matrix R in Eq. (27). The matrix R forms the input in the calculation of the *state* covariance matrix Q in Eq. (28) representing the errors $\Delta\mathbf{Z} = \mathbf{Z}^* - \mathbf{Z}$ in the optimal weighted-least-squares estimate of the attitude in Eq. (26a).

Discussion of Results Using Contour Data

The attitude determination technique presented earlier has been applied using sensor data produced by the CONTOUR spacecraft during its Earth-phasing orbits [3,4]. The data cover the 1 h midlatitude range (Fig. 2) during the Earth-sensor interval on 13 August 2002, two days before its ill-fated injection into an interplanetary trajectory [4]. The satellite's spin rate was close to 60 rpm, so that the 1 h batch of data contains about 3600 points.

Measurement Angles and Residuals

Figure 5 shows the actual as well as the predicted measurements of the half-chord angles. The predicted measurements are obtained by simulations involving the reconstruction of the sensor measurements (as in Fig. 2) based on the best available attitude estimate. The sensor data cover the 1 h interval starting at 36.6 h from perigee. This interval includes the midlatitude scans in between the two measurement singularities shown in Fig. 2 and therefore provides good-quality sensor measurements. Furthermore, the Earth sensor's scans are far away from the Earth's rim where the measurement biases of the chord lengths would become excessive.

The measurements in Fig. 5 point to the presence of significant biases in both half-chord angles. These are mainly caused by local and temporal variations in the Earth's infrared horizon. Figure 6 provides a clearer view of the residuals between the actual and expected measurements. The residuals reach the extreme value of over 0.3° in magnitude for the κ_1 residual at the start of the interval and taper off toward the end of the 1 h interval.

Figure 7 shows the Earth aspect angles derived from the measured half-chord angles in Fig. 5. The results designated as "Beta-1p" and "Beta-2m" refer to the applicable individual Earth aspect angle solutions β_1^+ and β_2^- after the sign ambiguity has been resolved. They are defined in Eqs. (12) in terms of the half-chord measurements κ_i ($i = 1, 2$). The "Average Beta" refers to $\beta_{\text{ave}} = (\beta_1^+ + \beta_2^-)/2$ and represents the most straightforward estimate of the Earth aspect angle.

The "Optimal Beta" in Fig. 7 is the minimum-variance estimate of the β angle obtained by the weighting technique of the two individual $\beta_i^\pm$ solutions outlined in Eqs. (15–21). As expected, this estimate gradually shifts from β_1^+, which has the lower variance during the first half of the interval, toward β_2^- with the lower variance in the second half.

Figure 8 shows the evolution of the residuals of the various β estimates shown in Fig. 7. These residuals represent the differences between the results in Fig. 7 (which are derived from the actual chord-angle measurements) and the reconstructed Earth aspect angles on the basis of the best available attitude estimate. The residuals clearly show the increases in the variances of the β measurements at the start and end of the interval, which are due to the magnification of the measurement noise in the vicinity of the singularities; see Figs. 3 and 4.

The important conclusion to be drawn from Figs. 7 and 8 is that the bias effects consistently dominate the random noise. The minimum-variance β solution shows good performance in reducing the random noise of the individual β_1^+ and β_2^- solutions. Unfortunately, this solution is not able to reconcile the large gap between the individual β angles induced by the bias effects. Over the shown interval, it gradually bridges the gap between the β_1^+ and the β_2^- solutions. On the other hand, the straightforward β_{ave} solution shows better overall performance in terms of its residuals.

Figure 9 shows the sun–Earth dihedral angle measurements α_i ($i = 1, 2$) generated by the Earth sensor's two pencil beams. The "Optimal Alpha" represents the average of the two angles α_1 and α_2 [Eq. (23)] because there is no obvious criterion for assigning different weights. The residuals of the three angles in Fig. 9 can easily be

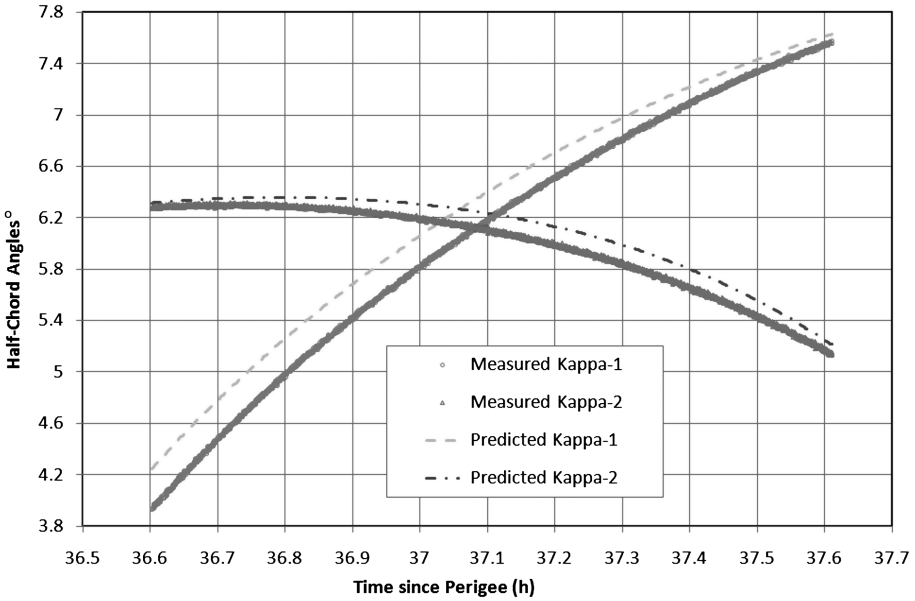

Fig. 5 Measured and predicted half-chord angles.

visualized after subtracting the "Predicted Alpha" shown in Fig. 9. The residuals of the Optimal Alpha start out with a magnitude of about 0.1°, pass through 0° at about 36.9 h, and settle down to a constant value of about −0.07°. Variations in the Earth's radiation profile, especially the north–south thermal gradient, are responsible for the systematic errors in the crossings of the Earth's infrared disk measured by the Earth-sensor detectors (see also [5]).

The evolutions of the sun aspect angle measurements and their residuals have been established as well (not shown here). The sun aspect angle varies only a little over the 1 h interval considered, that is, from 104.026 to 104.002°. The observed biases in the sun angle measurements are also relatively small and the residuals stay within a narrow range of about 0.01°.

Attitude Determination Results

The application of the T-S attitude determination technique to the CONTOUR sensor measurements shown in Figs. 5–9 produces the following optimal attitude estimate β^* in terms of its right ascension (RA) and declination (DE) angles:

$$\text{RA} = 258.593^\circ; \qquad \text{DE} = 29.199^\circ \tag{44}$$

This result is less than 0.05° in arc-length distance away from the fine attitude determination result given in Table 2 of [3].

The averages of the absolute residuals in the sun aspect angle ϑ, the Earth aspect angle β, and the sun–Earth dihedral angle α have been calculated by comparing the $N \approx 3600$ angular measurement sets with their corresponding predicted values reconstructed from the attitude estimate in Eq. (44):

$$\Delta\vartheta_{\text{res}} = (1/N)\Sigma_j|\vartheta_{j,\text{meas}} - \vartheta_{j,\text{pred}}| = 0.006^\circ \tag{45a}$$

$$\Delta\beta_{\text{res}} = (1/N)\Sigma_j|\beta_{j,\text{meas}} - \beta_{j,\text{pred}}| = 0.151^\circ \tag{45b}$$

$$\Delta\alpha_{\text{res}} = (1/N)\Sigma_j|\alpha_{j,\text{meas}} - \alpha_{j,\text{pred}}| = 0.052^\circ \tag{45c}$$

The $\Delta\beta_{\text{res}}$ in Eq. (45b) represents the average absolute value of the residuals shown in Fig. 8 based on the use of the Optimal Beta

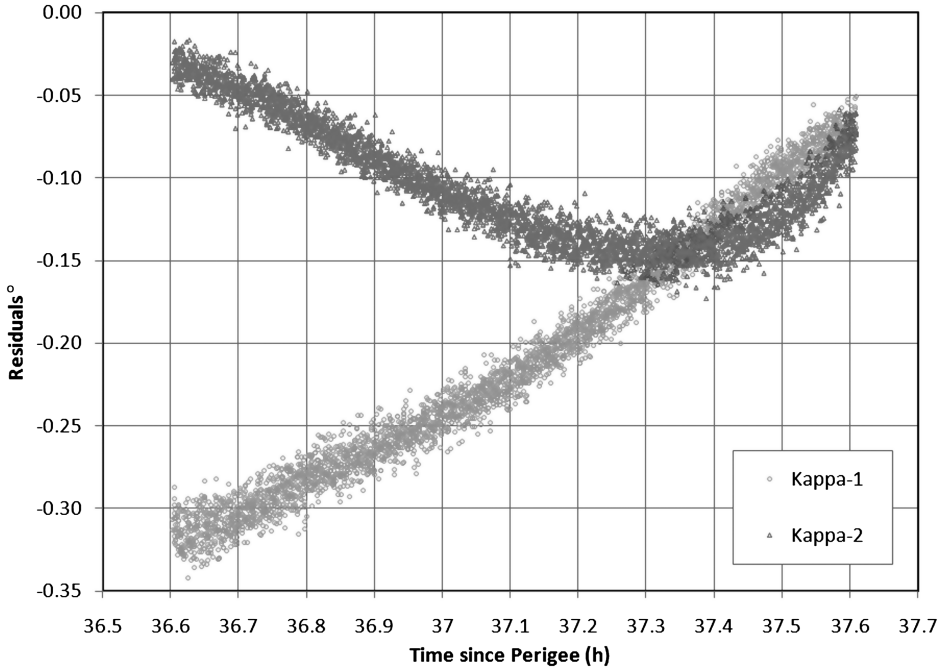

Fig. 6 Residuals of half-chord-angle measurements.

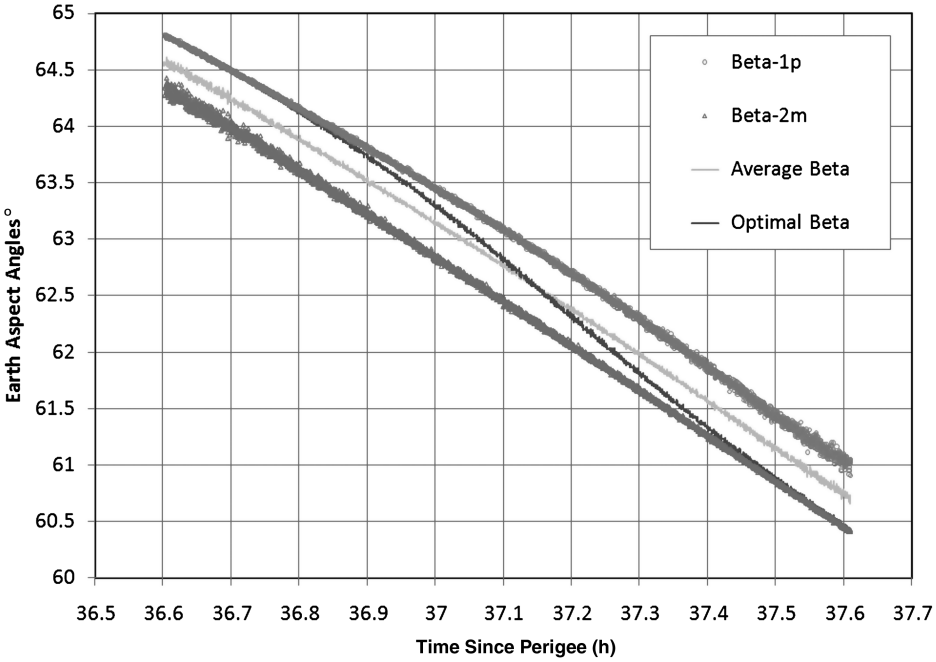

Fig. 7 Earth aspect angles derived from chord measurements.

estimate. As was mentioned earlier, the adoption of the Average Beta solution would lead to a lower residual, namely, 0.088°. This is a consequence of the detrimental effects of the biases in the half-chord measurements; see Figs. 5–8.

Figures 5–9 indicate that the effects of the measurement biases vary considerably over time. Therefore, it is of interest to investigate by how much the resulting attitude estimate varies over the interval under consideration. This approach allows us to compare the performances in terms of residuals of these local attitude estimates with those of the overall global estimate in Eq. (44). We recall that the optimal estimate given in Eq. (44) originates from the maximum-likelihood criterion in Eq. (2). It should be noted that this estimate is not necessarily optimal under the specific distance metric defined in Eqs. (45).

We performed a set of seven attitude determination runs over different 0.5 h intervals contained within the 1 h interval of data shown in Figs. 5–9. The interval for each run shifts by 5 min from the previous run, starting from 36.6 h from perigee. Thus, the first run uses the data from 36.6 to 37.1 h and the last (seventh) run uses those from 37.1 to 37.6 h.

Table 1 summarizes the results of the seven attitude determination runs. The second and third columns in Table 1 provide the RA and DE of the attitude estimates in degrees. The fourth column gives the angular deviation, that is, the arc-length distance, of the relevant attitude estimate from the overall optimal attitude estimate given in Eq. (44).

The final three columns of Table 1 summarize the averaged absolute residuals defined in Eqs. (45a–45c) in terms of the sun aspect angle (SAA), the Earth aspect angle (EAA), and the sun–Earth dihedral angle (SEDA), respectively. We emphasize that all residuals in Table 1 are computed with respect to the predicted measurements that are derived from the attitude estimate over the complete 1 h interval, that is, the estimate given in Eq. (44). It may be noted that each attitude estimate is optimal only within its own 0.5 h interval.

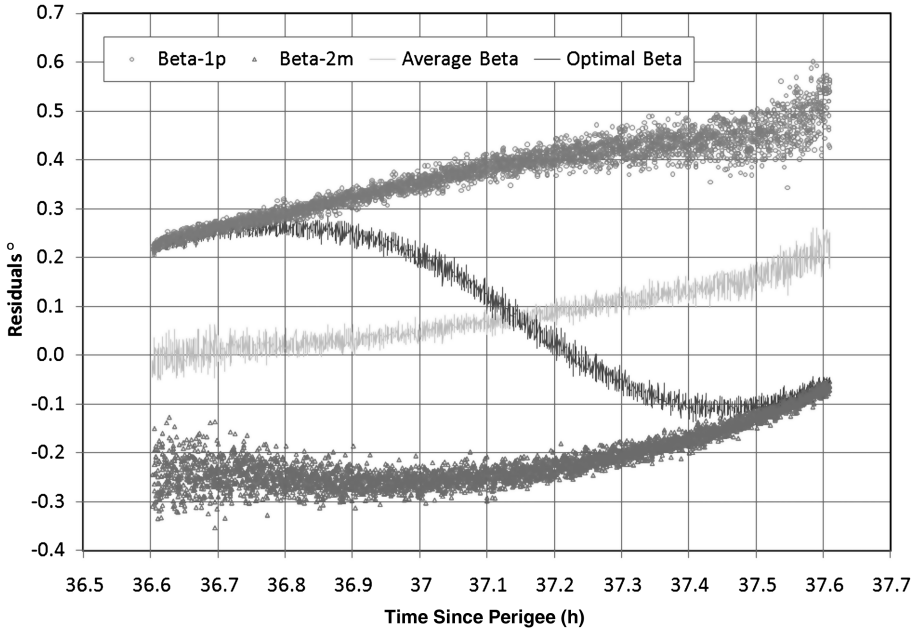

Fig. 8 Residuals of Earth aspect angle solutions.

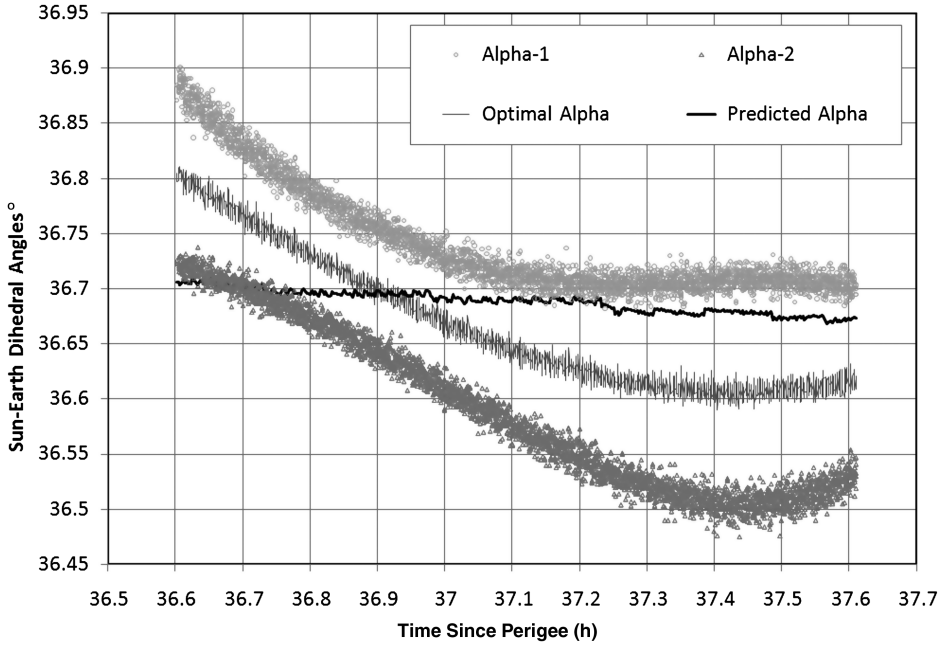

Fig. 9 Sun–Earth dihedral angle measurements.

Table 1 shows that all seven attitude results are less than 0.1° in arc length away from the overall attitude estimate in Eq. (44). Furthermore, the resulting average value of the attitude estimates listed in Table 1 is only 0.016 ° in arc length away from the overall result in Eq. (44). Also, the averages of the residuals are close to the ones of the overall estimate given in Eq. (45), which indicates that the results are consistent. When assuming that the deviations shown in Table 1 are normally distributed, we can calculate with a confidence level of 98.5% that the average attitude result is less than 0.1° away from the unknown actual attitude orientation.

Reconstruction of Earth-Radius Biases

When focusing on the residuals of the Earth aspect angle in Table 1, we find that they continually improve over the course of the interval. This trend is due to the peculiarities of the residuals in the S/E and E/S pulses. We recall that the Earth aspect angle is computed from the half-chord-angle measurements κ_i $(i = 1, 2)$ by means of the implicit Eq. (8). For simplicity we assume that the bias in the apparent Earth-radius angle ρ, which dominates all other biases, is the only bias acting over the interval. In this case, we can reconstruct the biases $\Delta\rho_i$ $(i = 1, 2)$ that produce the actually observed κ_i measurements. After linearization of the relationship in Eq. (8), we can express the reconstructed $\Delta\rho_i$ biases in the observed $\Delta\kappa_i$ residuals as follows:

$$\Delta\rho_i \approx \{\sin\mu_i \sin\kappa_i^* \sin\beta^* / \sin\rho_{\text{nom}}\}\Delta\kappa_{i,\text{res}} \qquad (i = 1, 2) \quad (46)$$

Table 1 Results of attitude determination runs for CONTOUR (all angles are in degrees)

	Attitude estimate			Residuals		
Run	RA	DE	Deviation	SAA	EAA	SEDA
1	258.648	29.286	0.099	0.0060	0.228	0.039
2	258.622	29.244	0.052	0.0063	0.201	0.034
3	258.598	29.205	0.008	0.0061	0.162	0.035
4	258.577	29.172	0.030	0.0061	0.130	0.042
5	258.559	29.145	0.062	0.0065	0.105	0.052
6	258.546	29.126	0.084	0.0063	0.087	0.060
7	258.539	29.116	0.096	0.0066	0.074	0.064
Average	258.584	29.185	0.062	0.0063	0.141	0.047
St. dev.	0.041	0.064	0.034	0.0002	0.058	0.012

where β^* and κ_i^* are the predicted measurements belonging to the overall attitude estimate in Eq. (44) and ρ_{nom} is the nominal Earth-radius angle, all as functions of time over the relevant interval.

Figure 10 shows the evolutions of the reconstructed $\Delta\rho_i$ $(i = 1, 2)$ biases as well as their mean value over the relevant interval. As expected, the evolutions of these biases mirror those of the associated half-chord angles shown in Fig. 6. Figure 10 indicates that the maximum bias in the apparent Earth-radius angle is of the order of 0.2°. This corresponds to a bias of about 210 km in the actually observed Earth's infrared radius compared to the predicted radius.

It can be seen that the $\Delta\rho_1$ bias is always larger in magnitude than $\Delta\rho_2$ but this difference decreases continuously over the interval. Furthermore, from about the middle of the interval, the magnitudes of both biases show a decreasing trend. It can be understood from Fig. 1 that a discrepancy between these two biases shifts the Earth aspect angle in proportion to the magnitude of the difference. Therefore, the decreasing discrepancy between these two biases over the interval considered is responsible for the continually decreasing $\Delta\beta$ residuals in Table 1.

Discussion of Results Using MSG-2 Data

The T-S attitude determination technique was also applied to sensor data produced by the MSG-2 satellite [5] at the end of its near-geostationary drift phase in December 2005. During the one-day data interval under consideration here, the spin-axis attitude was pointing in a direction about 3.5° away from the orbit normal. The spin rate was close to 100 rpm, which leads to a volume of about 140,000 sets of sensor measurements over the one-day interval. To limit the data volume to a manageable size, we performed a sliding averaging operation of the sensor measurements over 10 spin revolutions. Therefore, the measurement sampling interval increases to about 6.7 s and the attitude determination is performed on a batch of about 14,000 data points (compared to about 3600 points for CONTOUR).

Measurement Angles and Residuals

The MSG-2 Earth sensor's pencil beams are mounted at about 86 and 94 deg from the spin axis and provide continuous Earth coverage during normal-mode operations in the geostationary orbit. In the case considered here, that is, a near-geostationary orbit and an attitude pointing about 3.5° away from the orbit normal, the pencil beams have continuous Earth coverage with periodic (at orbit frequency) variations of the half-chord angles between about 4 and 9° [5].

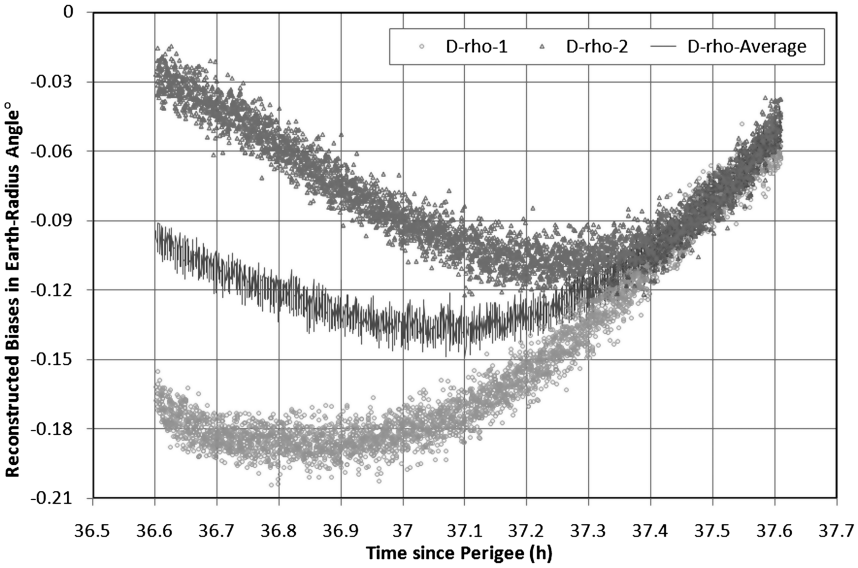

Fig. 10 Reconstructed biases in apparent Earth-radius angle.

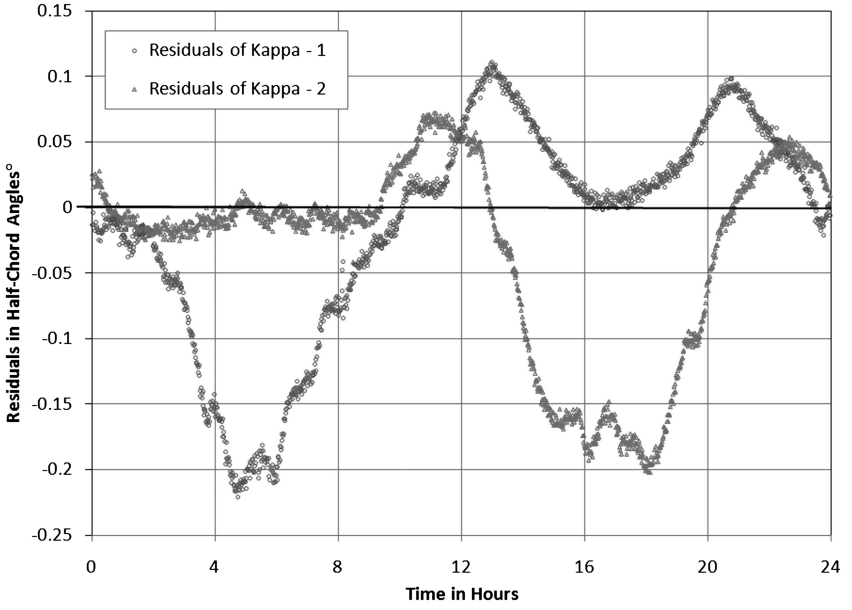

Fig. 11 Residuals of half-chord angles (MSG-2).

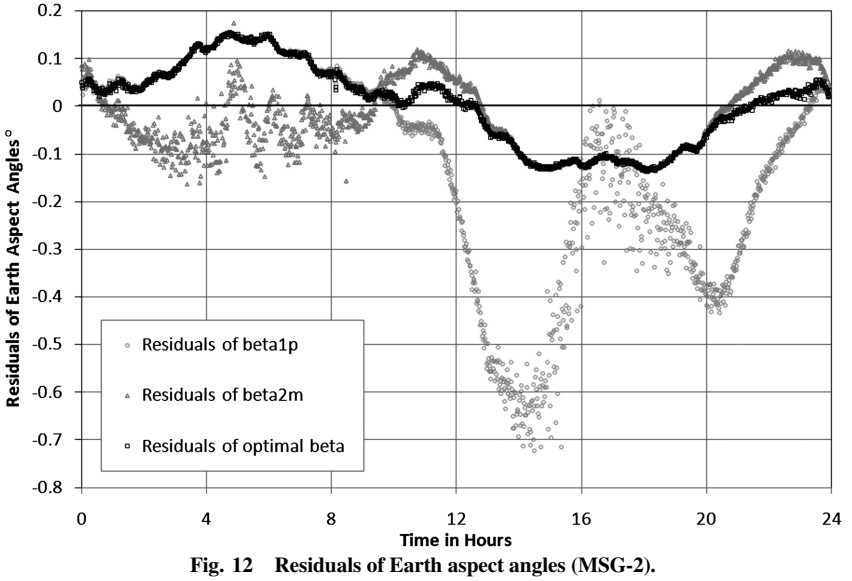

Fig. 12 Residuals of Earth aspect angles (MSG-2).

Table 2 Results of attitude determination runs for MSG-2 (all angles are in degrees)

	Attitude estimate			Residuals		
Run	RA	DE	Deviation	SAA	EAA	SEDA
1	83.358	86.522	0.014	0.0067	0.064	0.073
2	83.202	86.521	0.023	0.0065	0.062	0.088
3	83.585	86.529	0.002	0.0064	0.072	0.077
4	84.682	86.549	0.071	0.0065	0.107	0.059
5	84.575	86.551	0.065	0.0076	0.104	0.059
6	83.618	86.533	0.006	0.0070	0.074	0.076
7	83.084	86.525	0.029	0.0076	0.063	0.091
8	82.930	86.519	0.039	0.0067	0.058	0.096
9	83.619	86.524	0.005	0.0076	0.070	0.077
10	84.461	86.539	0.056	0.0073	0.097	0.053
11	84.185	86.535	0.038	0.0071	0.087	0.065
Average	83.754	86.532	0.032	0.0070	0.078	0.074
St. dev.	0.623	0.011	0.024	0.0005	0.018	0.014

Figure 11 shows the evolutions of the residuals of the half-chord angles κ_i $(i = 1, 2)$ over a one-day interval. The residuals are relatively large although they are somewhat smaller than in CONTOUR's case shown in Fig. 6. Also in this case, the residuals are mainly caused by variations in the Earth's infrared horizon. The largest deviations correspond to Earth sensor's scans close to the Earth's rim where the half-chord angles are relatively small, that is, below 5°. The smaller short-period ripples with an amplitude of 0.02–0.05° are caused by satellite wobbling effects induced by propellant imbalances between the tanks [5].

Figure 12 shows the residuals of the estimates of the Earth aspect angles based on the half-chord measurements. As before, the Beta-1p and Beta-2m results refer to the individual solutions β_1^+ and β_2^- and the Optimal Beta is the minimum-variance β angle obtained by the weighting technique of the $\beta_i^\pm$ solutions presented in Eqs. (15–21). Figure 12 does not show the Average Beta estimate β_{ave}, which can easily be visualized as the average value of the β_1^+ and β_2^- results.

As in the CONTOUR case, the minimum-variance estimate gradually shifts from the β_1^+ solution, which has the lower variance

Table 3 Effect of unit-vector normalization for CONTOUR (all angles are in degrees)

	Method		Attitude estimate			Residuals		
Run	EAA	Unit vector	RA	DE	Deviation	SAA	EAA	SEDA
1	Optimal	Yes	258.593	29.199	——	0.0061	0.151	0.052
2	Average	Yes	258.585	29.190	0.012	0.0043	0.088	0.049
3	Optimal	No	258.655	29.232	0.063	0.0015	0.139	0.045
4	Average	No	258.630	29.213	0.035	0.0015	0.049	0.045

Table 4 Effect of unit-vector normalization using only measurements ϑ, β for CONTOUR (all angles are in degrees)

	Method		Attitude estimate			Residuals		
Run	EAA	Unit vector	RA	DE	Deviation	SAA	EAA	SEDA
1	Optimal	Yes	258.685	29.378	0.196	0.0015	0.138	0.154
2	Average	Yes	258.650	29.315	0.126	0.0015	0.051	0.109
3	Optimal	No	260.302	38.277	9.187	0.0016	0.044	9.878
4	Average	No	257.875	25.491	3.763	0.0014	0.013	3.950

Table 5 Effect of unit-vector normalization for MSG-2 (all angles are in degrees)

	Method		Attitude Estimate			Residuals		
Run	EAA	Unit vector	RA	DE	Deviation	SAA	EAA	SEDA
1	Optimal	Yes	83.561	86.528	——	0.0064	0.071	0.131
2	Average	Yes	82.268	86.507	0.081	0.0067	0.097	0.168
3	Optimal	No	83.601	86.530	0.003	0.0064	0.072	0.130
4	Average	No	82.957	86.528	0.037	0.0065	0.095	0.148

Table 6 Effect of unit-vector normalization using only measurements ϑ, β for MSG-2 (all angles are in degrees)

	Method		Attitude Estimate			Residuals		
Run	EAA	Unit vector	RA	DE	Deviation	SAA	EAA	SEDA
1	Optimal	Yes	81.772	86.493	0.114	0.0066	0.060	0.184
2	Average	Yes	81.185	86.481	0.152	0.0066	0.106	0.202
3	Optimal	No	82.576	84.124	2.405	0.0065	0.022	0.172
4	Average	No	81.905	84.341	2.191	0.0065	0.086	0.191

Table 7 Convergence performances of unit-vector normalization technique

	CONTOUR		MSG-2	
Iteration	Three angles	Two angles	Three angles	Two angles
0	-1.2×10^{-3}	6.4×10^{-2}	5.4×10^{-6}	-3.1×10^{-3}
1	5.4×10^{-6}	1.3×10^{-2}	4.4×10^{-7}	1.8×10^{-5}
2	1.1×10^{-10}	6.5×10^{-4}	2.4×10^{-9}	-3.2×10^{-9}
3	7.8×10^{-16}	2.3×10^{-6}	6.8×10^{-14}	-3.8×10^{-9}

during the first half of the interval, to β_2, with the lower variance in the second half. The biases have a considerable effect on the optimal β with a maximum magnitude of the residual of about 0.15 deg. Nevertheless, the minimum-variance estimate clearly shows a better performance than the other three estimates in Fig. 12 by steering clear of the major biases, especially during the second half of the orbit.

In contrast with the CONTOUR case, the optimal β estimate has also a lower overall residual than the β_{ave} estimate, namely, $\Delta\beta_{\text{res}} = 0.071^\circ$ versus $\Delta\beta_{\text{ave}} = 0.096^\circ$ on the basis of the definition given in Eq. (45b).

Attitude Determination Results

The optimal attitude estimate β^* in terms of its RA and DE angles that is established from the full-day sensor measurements is

$$\text{RA} = 83.561^\circ; \qquad \text{DE} = 86.528^\circ \tag{47}$$

This result is only 0.04° in arc-length distance away from the European Space Operations Centre result given in [5]. The residuals, as defined in Eqs. (45), associated with the attitude estimate in Eq. (47) are

$$\Delta\vartheta_{\text{res}} = 0.0064; \qquad \Delta\beta_{\text{res}} = 0.071; \qquad \Delta\alpha_{\text{res}} = 0.078 \tag{48}$$

We performed a set of 11 attitude determination runs over 4 h intervals contained within the full day of MSG-2 data. The interval for each of the runs is shifted by 2 h from the previous run. Thus, the first run uses the sensor data from 0 to 4 h and the last run uses data between 20 and 24 h. The results are summarized in Table 2 with the same definitions as used in Table 1. The fourth column gives the deviation of the attitude estimate from the best overall estimate in Eq. (47) and the results of the residuals are based on the full 24 h interval.

The deviations between the attitude estimates listed in Table 2 and the overall result in Eq. (47) are relatively small in view of the significant biases. In particular, the attitude vector corresponding to the average RA and DE angles given in the last but one row of Table 2 is only 0.012° in arc length away from the overall attitude estimate in Eq. (47). The variations in the residuals over the 11 runs in Table 2 are also relatively small. Furthermore, all of the residuals in Table 2 are fairly consistent with those of the best attitude estimate in Eq. (48). When assuming that the deviations shown in Table 2 are normally distributed, we find with a confidence level of over 99% that the average attitude result is less than 0.05° away from the actual attitude orientation.

The average values and standard deviations of the residuals in the last two rows of Table 2 are mostly similar to those of the CONTOUR case in Table 1. However, the average attitude deviation and the average EAA residual are only about half the values of the values given in Table 1. This is expected to be due to the difference in size of the two data sets and the geometrical differences in the orbit and attitude conditions. Furthermore, the residuals are much more uniform in the present case and there is no clear trend over the course of the one-day interval.

Effects of Unit-Vector Normalization

Finally, we discuss the effect of the unit-vector normalization technique of the T-S algorithm with the help of the in-orbit sensor data for the two selected satellites.

Results for CONTOUR

Table 3 summarizes the results for the CONTOUR data set collected on 13 August 2002. The second column refers to the selection of the EAA, that is, the optimal β^* or the average β_{ave}. The third column specifies whether the unit-vector normalization was performed or not. The remaining columns are defined as in Tables 1 and 2 except that the deviation is calculated relative to the attitude estimate in the first row, which is expected to be the most precise.

The results of runs 1 and 2 are very close but the results of run 2 have smaller residuals, especially for the Earth aspect angle, which is consistent with the results shown in Figs. 6 and 7. Runs 3 and 4 do not use the unit-vector normalization technique but the results remain fairly close to those in runs 1 and 2, whereas the residuals are even lower. The latter makes sense because the optimization process is not restrained by the unit-vector condition.

It should be noted that the four runs in Table 3 use the full set of three measurement angles, ϑ, β, and α, which provides some robustness to the attitude estimates, even in the presence of significant biases. If the sun–Earth dihedral angle α measurement were not available, the component of the attitude vector normal to the plane formed by the sun and the Earth vector would have a relatively large error under the measurement biases.

Table 4 illustrates the benefit of the unit-vector normalization procedure in the case in which the sun–Earth dihedral angle is not available. The performances of runs 1 and 2, which use the unit-vector normalization, are within 0.20° in arc-length distance from run 1 in Table 3. On the other hand, runs 3 and 4, which do not use the normalization technique, have unacceptably large errors of many degrees.

Results for MSG-2

Table 5 summarizes the results for the MSG-2 data set with the same definitions as in Table 3. The difference between the optimal and average estimates of runs 1 and 2 is larger than in the CONTOUR case but run 1 has the smaller residuals; see also Fig. 12. Runs 3 and 4 do not use the unit-vector normalization technique but the results remain very close to those in runs 1 and 2 and also the residuals are similar or somewhat smaller.

Table 6 illustrates the benefit of the unit-vector normalization procedure in the case in which the sun–Earth dihedral angle is not available. The performances of runs 1 and 2, which use the unit-vector normalization, are within 0.16° in arc-length distance from run 1 in Table 5. Runs 3 and 4, which do not use the normalization technique, have very large errors of over 2 deg, whereas their residuals are lower than those in runs 1 and 2, as expected.

Convergence of Iterations

Finally, we summarize the convergence performances of the normalization technique for the applicable runs in Table 7. The numbers shown are the differences of the magnitudes of the estimated attitude vector compared to unity, that is, $|\mathbf{z}| - 1$. The performances are excellent for the runs that use all three measurement angles for both CONTOUR and MSG-2, that is, columns 2 and 4. We find values for the deviations from unity of the order of 10^{-6} after just one iteration and about 10^{-9} after two iterations for both satellites. In the cases in which only two measurement angles (ϑ and β) are taken into account, that is, columns 3 and 5, the convergence performance is considerably slower, especially in the CONTOUR case.

Conclusions

The Tanygin–Shuster method for spin-axis attitude determination has been applied to in-orbit sensor data generated by two satellites,

namely, CONTOUR in a highly elliptical Earth-phasing orbit and MSG-2 in a near-geostationary orbit. The results indicate that the method produces stable attitude estimates for both satellites even in the presence of severe unknown biases. The unit-vector normalization technique is beneficial for the stability of the attitude determination results, especially in the case in which the dihedral angle measurements are not used.

References

[1] Shuster, M. D., "Efficient Algorithms for Spin-Axis Attitude Estimation," *The Journal of the Astronautical Sciences*, Vol. 31, April–June 1983, pp. 237–249.

[2] Tanygin, S., and Shuster, M. D., "Spin-Axis Attitude Estimation," *The Journal of the Astronautical Sciences*, Vol. 55, No. 1, 2007, pp. 107–139.

[3] Van der Ha, J., Rogers, G., Dellinger, W., and Stratton, J., "CONTOUR Phasing Orbits: Attitude Determination and Control Concepts and Flight Results," *Advances in the Astronautical Sciences*, Vol. 114, Pt. 2, 2003, pp. 767–781.

[4] Dunham, D. W., Muhonen, D. P., Farquhar, R. W., Holdridge, M., and Reynolds, E., "Design and Implementation of CONTOUR's Phasing Orbits," *Advances in the Astronautical Sciences*, Vol. 114, Pt. 3, 2003, pp. 1535–1548.

[5] Van der Ha, J. C., and Janssens, F. L., "Spin-Axis Attitude Determination from Earth Chord-Angle Variations for Geostationary Satellites," *Journal of Guidance, Control, and Dynamics*, Vol. 32, No. 5, Sept.–Oct. 2009, pp. 1598–1608. doi:10.2514/1.40752

[6] van der Ha, J. C., "Spin Axis Attitude Determination Accuracy Model in the Presence of Biases," *Journal of Guidance, Control, and Dynamics*, Vol. 29, No. 4, July–Aug. 2006, pp. 799–809. doi:10.2514/1.17745

[7] Markley, F. L., and Sedlak, J. E., "Kalman Filter for Spinning Spacecraft Attitude Estimation," *Journal of Guidance, Control, and Dynamics*, Vol. 31, No. 6, Nov.–Dec. 2008, pp. 1750–1760. doi:10.2514/1.35221

[8] Wertz, J. R. (ed.), *Spacecraft Attitude Determination and Control*, Springer Scientific + Business Media, Berlin/New York, 1978.